Magneto-Inductive Tracking in Underground Environments

Traian E. Abrudan, Orfeas Kypris, Niki Trigoni, Andrew Markham

1. Introduction

GPS has revolutionized outdoor navigation and tracking, providing highly accurate positioning anywhere in the world. However, as it uses high frequency radio waves, it suffers heavily from multipath and attenuation effects that are caused by buildings, thick vegetation and is completely unusable underground. There is a strong need to be able to position people, equipment and assets in underground environments without resorting to manual surveying. In this chapter, we discuss how positioning in GPS-denied environments can be accomplished by using low-frequency magnetic fields. These fields have the special property of being able to penetrate most natural media without further attenuation and due to their long wavelengths, do not suffer from multipath effects. However, the generation and detection of magneto-inductive fields is challenging which has limited their uptake. This chapter discusses applications where they have been successfully used and provides an overview of the fundamental approaches to positioning in single and multi-hop scenarios. Finally, it concludes by outlining challenges and limitations.

1.1. Approaches to GPS-Denied Tracking

High frequency radio propagation suffers from multipath and attenuation in underground tunnels. In particular, RF cannot penetrate more than a few cm of soil/rock, limiting its use to line-of-sight (LOS) scenarios. This in turn means that a network for positioning in underground mines using RF typically needs to be relatively dense to maintain a high proportion of LOS paths. A number of researchers (e.g. Huang et al. (2010)) have attempted to transfer localization techniques which work relatively well in above-ground scenarios to underground environments. One of the most common techniques is the use of Zigbee or WiFi based RSSI measurements. Cypriani et al. (2015) used WiFi measurements in a 70 m underground mine to demonstrate that mean errors in the order of 10 m were possible using RSSI measurements. Their innovations included the use of "capture points" to continually measure channel properties and variations. However, the major limitation with this approach is that the 90% positioning errors exceeded 25 m. Zigbee based time-of-flight measurements in underground tunnels were presented in Bedford and Kennedy (2012), which showed that acceptable ranging errors in the order of a 10 m could be obtained in linear tunnels of lengths up to 200 m. However, the trials were conducted in straight tunnels - performance around corners was not tested. Ultra wideband (UWB) has also been proposed as a means for positioning in underground mines, as it can achieve excellent (cm-level) accuracy in many indoor environments. Nkakanou et al. (2011) obtained UWB measurements in an underground mine and showed that for the LOS case, path loss was around 1.8, whereas for non-line of sight, path loss increased greatly to an exponent of 4.0. Similarly the RMS delay spread

increased from 1ns to 4ns over a range of only 10 m. The delay spread is caused by arrival of multiple delayed impulses, caused by the rough tunnel surface and reflections.

Other options that have been explored include geomagnetic positioning (Haverinen and Kemppainen (2011); Park and Myung (2014)), laser map-matching (Shaffer et al. (1992)), seismic waves (Squire et al. (2009)), acoustic techniques (Pfeil et al. (2015)) and dead-reckoning (Hawkins et al. (2006)). Acoustic positioning has been used for precise underground positioning next to large machinery, as in Pfeil et al. (2015). Again, however, this technique is LOS based and requires signals from four non-colocated sources to determine the location of the receiver. Optical based techniques, both based on natural mine features and deployed landmarks can provide superior positioning accuracy in the order of a few cm. Apart from being LOS, their main limitation is continuous operation in dusty environments. Geomagnetic positioning is a form of spatial fingerprinting that relies on distortions of the Earth's magnetic field that are caused by metal objects and rocks. With the aid of a good fingerprinting database, it was shown that accuracies in the order of a few metres were obtainable in an extremely deep (1400 m) mine (for details, refer to Haverinen and Kemppainen (2011)). The major advantage of this modality is that it is infrastructureless and relies simply on the pre-existing magnetic field distortions. However, its drawbacks of requiring an accurately surveyed fingerprint map, and the need to travel a relatively long distance (ca. 35 m) to localize the target limit its widespread adoption.

1.2. Magneto Inductive Technology

There is one wireless technology that has the property of being able to penetrate most naturally found materials (soil, water, rock etc.) with minimal loss, namely magneto-inductive (MI) technology. MI at the scale in underground mines refers to very low frequency (VLF) fields (wavelengths of hundreds of metres or even kilometres). At these wavelengths, the energy is virtually entirely contained within the quasistatic magnetic field and inductive coupling occurs between source and sensor. The field itself is non-propagating and non-radiative. As such, it cannot suffer from multipath, and attenuation of signal is primarily due to the magnetic permeability of the media through which it passes.

MI communication has had a long history of use in underground environments (see Yarkan et al. (2009) for a comprehensive overview of different underground communication technologies). This was first proposed by Tesla in 1896, although the first real through-the-earth (TTE) communication system was presented by Wadley (1946) in 1946 in a mine in South Africa. A VLF based system was shown by Barkand et al. (2006) which allowed for audio transmission through approximately 100 m of overburden. The drawback of this system was the large size of the antennas, requiring a 20 m loop to be laid out to perform communication. An interesting approach to mine communication is to exploit the large amount of metal rails and wiring to promote signal propagation in the medium field (MF) band (Stolarczyk (1991)). These conductors act as waveguides, allowing for far more efficient propagation than through solid media. MI has also been used as a communication modality for wireless underground sensor networks (e.g. see Sun and

4

Akyildiz (2010)) for applications such as precision agriculture, as opposed to high-frequency RF based propagation (e.g. see Silva and Vuran (2009); Stuntebeck et al. (2006)). To overcome the issues with high path loss, a novel passive waveguide scheme was proposed in Sun and Akyildiz (2010) where intermediate passive resonant loops act as flux concentrators. This helps to reduce the overall path loss, at the cost of a loss in omnidirectionality. A multi-hop MI based communication system, which helps to address some of the scale limitations of single hop devices was presented in Markham and Trigoni (2012a). This employed triaxial antennas, in contrast to earlier work which used single axis antennas. The advantages of using triaxial antennas in a communication system are two-fold: firstly, antennas do not need to be oriented carefully with respect to one another, and secondly, a novel encoding scheme, termed magnetic vector modulation, can be used to nearly triple the achievable data rate without incurring a power or bandwidth penalty.

MI positioning, which involves measuring characteristics of the established field, has been relatively well researched in a number of areas, including virtual reality and medical positioning. Typically, the focus of these developments has been on very high accuracy (mm) over short ranges (3 m). The seminal paper by Raab et al. (1979) presented a 3-D positioning system that could use a single three-axis (triaxial) source to determine both the position and orientation of a triaxial sensor. The key innovation was treating the received signals as three-dimensional vectors with both sign and magnitude. By doing so, they demonstrated that by using spatial transformations and coordinate rotations that the position and orientation of the receiver could be determined by treating the source as three orthogonal dipoles. This was a key

insight that provided one of the first motion-capture systems. In particular, MI positioning has found widespread use in medical applications, as it can provide mm level accuracy for guiding catheters and other instruments inside the human body (Hummel et al. (2005)). One of the issues that faces MI positioning systems in medical applications is the large amount of distorting (metallic) material that is typically found in an operating theatre. This in itself has led to a number of studies investigating calibration techniques (e.g. see Kindratenko (2000)) to reduce or mitigate distorted positions. Underground MI positioning is a relatively new area of exploration - in this chapter, we outline some recent work in this field and its applications, ranging from positioning in caves to tracking animals underground.

2. Channel Model

The channel relates how transmitted signals appear at a spatially displaced and possibly rotated receiving antenna. It relates how much energy from the transmitter arrives at the receiver and characterizes the impact of the media where the quasistatic signal has been established.

2.1. Source

A magneto-inductive source is created by modulating the current passing through a coil, generating a magnetic moment. The magnitude of the magnetic dipole moment of a magneto-inductive source is given by

$$m = NIA, \tag{1}$$

where N is the coil number of turns, I is the current passing through the coil, and A is the coil cross-sectional area. Transmitting coils are typically

air-cored as most permeability enhancing materials (e.g. ferrite) saturate under high magnetic fields. It can be seen from Eq.(1) that for a given cross-sectional former area, the moment can be increased either by adding more turns or increasing the current. Note however, that for a given wire gauge, these are coupled parameters - increasing the number of turns increases the coil resistance, which makes it more challenging to drive the same amount of current through the coil. Fundamentally, the magnetic moment is thus related to the mass of copper (or other conductor) used to make the transmitting antenna.

This can be shown as follows: consider the DC resistance R of a coil with N turns and circumference l:

$$R = \frac{Nl}{\sigma A} \tag{2}$$

where A is the cross-sectional area of the wire. At higher frequencies, where the skin effect becomes significant, one must replace A with the effective cross-sectional area $A_{\text{eff}} \simeq \pi \delta d$, where δ is the skin depth, and d is the wire diameter; this substitution gives the AC resistance. The complex impedance Z of the coil is defined as

$$Z = R + j\omega L - \frac{j}{\omega C} \tag{3}$$

where L and C are the inductance and capacitance of the coil respectively. When the coil is tuned to resonance such that $\omega = 1/\sqrt{LC}$, the imaginary part disappears and we are only left with the real part, R. At low frequencies, the current I flowing through the circuit due to an applied voltage V_{p} will thus be equal to

$$I = \frac{V_{\mathrm{p}}}{R} = \frac{V_{\mathrm{p}}\sigma A}{Nl}. \tag{4}$$

The loop area of a circular coil is given by $A_l = l^2/2\pi$. Thus, the generated magnetic moment in a coil of N turns with a loop area A_l due to a current I will be

$$m = NIA_l = \frac{V_p\sigma Al}{4\pi} \tag{5}$$

which simplifies to

$$m = \frac{V_p\sigma}{4\pi}V = \frac{V_p\sigma\rho_m}{4\pi}m_1 = km_1 \tag{6}$$

where V is the volume of one turn of wire, ρ_m is the mass density of the conducting material, $k = \frac{V_p\sigma\rho_m}{4\pi}$ is a constant that incorporates applied voltage, coil geometry and conductor properties, and m_1 is the mass of one turn of wire. Therefore, given a constant applied voltage, and provided the frequency is low enough such that $\delta \gg d/2$, *the generated magnetic moment is linearly dependent on the mass of one turn of conducting material.* The reason why the moment does not increase with N is because increasing the turns also increases the total resistance of the coil, which has a counterbalancing effect.

A simple calculation for determining when this relationship is true can be performed as follows: consider a copper coil with electrical conductivity $\sigma = 5.96 \times 10^7$ S/m, magnetic permeability $\mu = \mu_0 = 4\pi \times 10^{-7}$ H/m, operating at a frequency of $f = 100$ kHz, and with a wire diameter d of 0.2032 mm (corresponding to AWG 32 wire). The skin depth will be

8

$$\delta = \sqrt{\frac{2}{\sigma\omega\mu}} = 0.20616 \text{ mm} \tag{7}$$

— Since $\delta \gg d/2$, we conclude that the relationship of (6) holds. In fact, to make efficient use of the mass of conducting material, *we must have $\delta \gg d/2$,* to ensure that at the chosen operating frequency the current density is as uniform as possible over the cross sectional area of the wire.

The turns of the antenna cause it to act as an inductor, with a reactive impedance at the driving frequency. To increase efficiency, the coil is coupled with a tuned capacitor to make it resonate at the desired carrier frequency. At resonance, the complex impedance of the loop inductor and tuning capacitor cancel each other out, leaving the coil resistance as the effective impedance of the loop. To yield a high magnetic moment, the coil resistance should be as low as possible, which makes the antenna quality factor (Q) high. However, a very high Q leads to a limited transmitter bandwidth and high sensitivity to component tolerances and variation. It can be seen from this that the optimal design of a transmitting antenna depends on a number of factors and great gains in performance can be made by matching the requirements of the system to the constraints on the antenna.

Limits are set on the maximum allowable magnetic moment, both for health and safety of humans and also for compliance to intrinsic safety standards. The allowable limits depend on the frequency, as at higher frequencies, currents are induced more easily in conductive tissue. Guidelines for maximum magnetic moment set by ICNIRP are shown in Table 1, which are set by the reference distance. Using a reference distance of 1 m, it can be seen that at a frequency of 2.5 kHz, the maximum (safe for human exposure)

9

magnetic moment is 320 Am^2.

Frequency	E (kVm^{-1})	H (Am^{-1})	B (T)	m (Am^2) @ 1 m	m (Am^2) @ 10 m
50 Hz - 400 Hz	2.5×10^2/f	1.6×10^2	2×10^{-4}	2×10^3	2×10^6
400 Hz - 3 kHz	2.5×10^2/f	6.4×10^4/f	8×10^{-2}/f	8×10^5/f	8×10^8/f
3 kHz - 10 MHz	8.3×10^{-2}	21	2.7×10^{-5}	2.7×10^2	2.7×10^5

Table 1: Reference levels for the electric field strength E, magnetic field strength H, and magnetic flux density B, for general public exposure to time-varying electric and magnetic fields (unperturbed rms values). Transmitter magnetic moment m was calculated from B, assuming that the reference level is set at a 1 m and 10 m distance from the transmitting magnetic dipole. Adapted from International Commission on Non-Ionizing Radiation Protection (2010)

2.2. Impact of media

A quasistatic magnetic field is established in the surrounding material by the source. When operating in air, the relative coefficient of permeability of air, μ_r, is virtually unity, so there is insignificant deviation between the free-space model and this setup. However, in dense media, such as rock and soil, there are two factors that can alter the strength of the field sensed at the receiver. The first is the relative permeability and the second is the conductivity of the material. The relative permeability for most non-ferromagnetic materials is very close to 1, so this effect is typically negligible. However, the conductivity of the material can have a major impact on the establishment of the field as the time-varying magnetic field induces a current in the media which acts to oppose the primary field. This can cause rapid attenuation of the magnetic field and consequent reduction in range.

The relative permeability μ_r of biological mass is very close to one, and the same is valid for air and water. This fact is important, as absorption by people is not only detrimental to positioning, it can also carry safety risks.

10

Water is frequently encountered in underground mines, and thus the ability to penetrate water with little attenuation is essential. Most rocks, silt and clay have a relative permeability is very close to one. The work by Telford et al. (1990) addresses the magnetism of rocks and minerals, and point out that magnetically important minerals are surprisingly few in number. Except for magnetite, pyrrhotite and titanomagnetite, all the other minerals have $\mu_r \approx 1$. In conclusion, since most soils in nature do not contain magnetite, we can safely assume that the relative permeability of most underground environments is close to one.

Concerning conductivity, most dry rocks have very low conductivity. However, when the water content increases, the conductivity may also increase. Most minerals possess high conductivity, except for some compounds that contain iron, copper, and other metals. In order to quantify the penetration capabilities of the magnetic field, we provide in Table 2 skin depth calculations for various classes of rocks and minerals. These are pessimistic, assuming very high water concentrations, which is not typically the case in underground environments. Two different frequencies are considered: 2.5 KHz (used for localization in e.g. Abrudan et al. (2015); Markham and Trigoni (2012a)), and 10MHz (used for communication in Sun and Akyildiz (2010)). The skin effect is substantially higher at higher frequencies due to the contribution of the conductivity, and therefore, the secondary field will be significant, which leads to deviations from the magnetic dipole, and to higher attenuation with the distance. The table demonstrates that although the permeability of most media is close to unity, the conductivity can have a much greater impact on achievable range.

Material	Skin depth [m] (f = 2.5 KHz)	Skin depth [m] (f = 10 MHz)
Natural waters (ign. Rocks)	30.20	0.48
Natural waters (sediments)	3.90	0.06
Sea water	10.07	0.16
Ice	≥ 100	≥ 100
Surface waters(ign. Rocks)	3.18	0.05
Surface waters(sediments)	31.83	0.62
Clays	10.07	0.16
Schists (calcareous and mica)	45.02	0.75
Conglomerates	≥ 100	11.50
Sandstones	10.07	0.16
Limestones	71.18	1.25
Granite	≥ 100	56.29
Slates (various)	≥ 100	8.03
Bitum. Coal	7.80	0.12
Hematite	0.58	0.01
Pyrite	0.05	0.00
Pyrolusite	0.71	0.01
Pyrrhotite	0.45	0.01
Titanomagnetite	0.08	0.00
Magnetite	0.45	0.01

Table 2: The minimum skin depth for some different rocks and minerals at two different frequencies: 2.5KHz and 10 MHz

2.3. Receiver

Although magnetic sources typically comprise coils of conductive wire, there are many more approaches to sensing magnetic fields, with different size, weight, power and cost implications. The simplest sensor is the humble coil, which senses alternating magnetic fields by their induced voltage. Tumanski (2007) shows that the SNR of the air cored coil is governed primarily by the diameter of the core. This intuitively makes sense from the fact that a larger cross-sectional area will intersect more flux lines, creating a higher signal compared to the self-noise of the sensor. To reduce the size of receiving antennas, a material with high permeability (e.g. metglas) can be used as a core, at the cost of linearity and increased noise. The voltage output from the coil is related to the rate of change of the magnetic flux, so inherently has a frequency dependence. This can be integrated (either with an analog circuit or digitally) to provide a flat, wideband response. Solid state sensors based on hall or magneto-resistive properties of semiconductors can provide reasonable sensitivity, but in small packages. The gold-standard for ultra-high sensitivity remains the SQUID (super-cooled quantum inference device) sensor. However, such sensors are expensive and bulky. For a very comprehensive overview of magnetic sensing technology, refer to Tumanski (2007).

2.4. Channel Model

In this section, we provider a simple model to predict the spatial distribution of the magnetic field in an undistorted environment. Consider a triaxial transmitter located at $(x, y, z) = (0, 0, 0)$ and a receiver located at $\mathbf{r} = (x_r, y_r, z_r)$. The range between the transmitter and receiver is $r = \|\mathbf{r}\|_2$.

We consider generating a signal on three mutually orthogonal antenna, which we term a *triaxial* transmitter. In practice, this can be accomplished by sequentially energizing each coil in turn (time-multiplexing) or using a different frequency for each coil (frequency-multiplexing). As will be shown later, the use of triaxial antennas at both transmitter and receiver conveys unique advantages for positioning and tracking. Let us consider a triaxial whose X, Y, Z coils are subsequenctly energized. The magnetic moments corresponding to the three axes are:

$$\mathbf{m}_i = N_{\mathrm{TX}} I_{\mathrm{TX}} A_{\mathrm{TX}} \mathbf{e}_i, \tag{8}$$

where N_{TX} is the coil number of turns, I_{TX} is the current through the coil, A_{TX} is the cross-sectional area of the transmitter coil, and $\mathbf{e}_i$, $i = 1, 2, 3$ are the excitation versors corresponding to the standard Euclidean basis vectors.

Considering a generic magnetic moment vector $\mathbf{m}$, the magnetic field flux density at position $\mathbf{r}$ may be expressed using the magnetic dipole equations as:

$$\mathbf{B}(\mathbf{r}, \mathbf{m}) \quad = \quad \frac{\mu_{\mathrm{TX}}}{4\pi} \left[\frac{3\mathbf{r}(\mathbf{m}^T \mathbf{r})}{r^5} - \frac{\mathbf{m}}{r^3} \right] = \frac{\mu_{\mathrm{TX}}}{4\pi r^3} \left[\frac{3\mathbf{r}\mathbf{r}^T}{r^2} - \mathbf{I}_3 \right] \mathbf{m}, \tag{9}$$

where μ_{TX} is the transmitter coil core magnetic permeability, $\mathbf{I}_3$ is the 3-by-3 identity matrix, and $(\cdot)^T$ denotes the matrix transpose operation. Given the three mutually perpendicular the magnetic moments $\mathbf{m}_i$, $i = 1, 2, 3$ in Eq. (8), we obtain the corresponding magnetic field flux density vectors $\mathbf{B}_i = \mathbf{B}(\mathbf{r}, \mathbf{m}_i)$.

Let $\mathbf{\Omega}_t$ be a 3-by-3 orthogonal matrix whose columns represent the axes of the triaxial receiver in the transmitter frame. Grouping the $\mathbf{B}_i$ column vectors in a matrix $\mathbf{B}_{1,2,3} = [\mathbf{B}_1, \mathbf{B}_2, \mathbf{B}_3]$, the magnetic field can be expressed

14

as:

$$\mathbf{\Omega}_\mathrm{t}^T \mathbf{B}_{1,2,3} = \frac{\mu_\mathrm{TX} N_\mathrm{TX} I_\mathrm{TX} A_\mathrm{TX}}{4\pi r^3} \mathbf{\Omega}_\mathrm{t}^T \left[\frac{3\mathbf{r}\mathbf{r}^T}{r^2} - \mathbf{I}_3\right] \underbrace{[\mathbf{e}_1, \mathbf{e}_2, \mathbf{e}_3]}_{\mathbf{I}_3,} \tag{10}$$

Each excitation $\mathbf{e}_i$ at TX will induce a voltage on the ith receiver axis, which may be represented by a 3-by-1 vector

$$\mathbf{v}_i \propto 2\pi f \mu_\mathrm{RX} N_\mathrm{RX} A_\mathrm{RX} \mathbf{\Omega}_\mathrm{t}^T \mathbf{B}_i, \tag{11}$$

where f is the excitation carrier frequency, N_RX is the receiver coil number of turns, and A_RX is the receiver coil cross-sectional area. The energy transfer between transmitter and receiver triaxial coils can be modeled as a 3×3 MIMO channel matrix $\mathbf{S}$ given by

$$\mathbf{S} \triangleq [\mathbf{v}_1, \ \mathbf{v}_2, \ \mathbf{v}_3], \tag{12}$$

whose ith column $\mathbf{v}_i$ is given in Eq. (11). The three excitations correspond to a space-time code whose coding matrix is $\mathbf{I}_3$ (see Eq. (10)). Combining Eqs. (10)–(12), we can write

$$\mathbf{S} = c\mathbf{\Omega}_\mathrm{t}^T \left[\frac{3\mathbf{r}\mathbf{r}^T}{r^2} - \mathbf{I}_3\right]. \tag{13}$$

The elements $s_{j,i}$ of the MIMO channel matrix $\mathbf{S}$ are proportional to the voltages induced from the ith TX coil to the jth RX coil. The scaling constant decays with the third power of range, i.e., $c \propto 1/r^3$. Note that the matrix $\mathbf{S}$ contains the 3-D RX position $\mathbf{r}$ and orientation $\mathbf{\Omega}_\mathrm{t}$ which we are interested in.

3. Single Hop Localization

In this section, we describe how, given the channel model, we can derive the positions and orientations of a receiver. A major advantage of using

triaxial antennas at source and receiver is that a single source can be used to localize a receiver in 3-D. This is in stark contrast to conventional range based systems which require four or more non-colocated anchors to estimate 3-D position. This result arises from the property that the magnetic field is a vector field i.e. it has both magnitude and direction. Fundamentally, if one considers the equation for the flux Φ passing through a coil with area A:

$$\Phi = \mathbf{BA} = BA\cos(\theta), \tag{14}$$

it can be seen that there is an angular dependence between the voltage sensed and the generated magnetic field. This property is exploited to provide positioning information as described below.

The channel matrix $\mathbf{S}$ may be used to estimate the position the receiver in 3-D, subject to a hemispherical ambiguity, which is inherent, due to the symmetry of the dipole magnetic field. Therefore, the estimated position corresponds to either (x_r, y_r, z_r), or $(-x_r, -y_r, -z_r)$. This ambiguity may be using map information, inertial measurements, or multiple transmitters. The rest of this section addresses the single transmitter magneto-inductive 3-D positioning. First, we estimate the range from the total received power, which corresponds to the Frobenius norm of the MIMO channel matrix. Then, we can then compute the bearing angles (azimuth and elevation) from the eigendecomposition of channel matrix.

Range Estimation The Frobenius norm of $\mathbf{S}$ defines the total received power, and in undistorted environments, it follows an inverse-cube law

$$\|\mathbf{S}\|_{\mathrm{F}} \propto r^{-3}. \tag{15}$$

16

Since Frobenius norm is invariant to orthogonal transforms, the range is also invariant with respect to the relative orientation of the traxial transmitter and receiver. This is an important factor, as the orientation of the receiver is difficult or impossible to keep constant in a number of underground applications. Let us define the total Received Signal Strength Indicator (RSSI) measured in dB as

$$\rho \triangleq 20 \lg \|\mathbf{S}\|_\mathrm{F}. \tag{16}$$

Due to the inverse cube law of the magnetic filed decay, the RSSI at distance r can be expressed as

$$\rho = \rho_0 - 60 \lg(r/r_0), \tag{17}$$

given the RSSI ρ_0 measured at reference distance r_0 (determined by calibration). Thus, the transmitter-receiver distance may be estimated as

$$r = r_0 10^{(\rho_0 - \rho)/60}. \tag{18}$$

Position estimation Knowing the range, we still need to determine the direction of the position vector $\mathbf{r}$ in 3-D, i.e., the position versor $\mathbf{u} = \mathbf{r}/r$. We first need to get rid of the orientation information. Let us define the matrix

$$\mathbf{C} = \mathbf{S}^T \mathbf{S}. \tag{19}$$

According to Eq. (13) the orientation cancels out in Eq. (19). Therefore, $\mathbf{C}$ is orientation invariant and may be used to estimate the 3-D position versor $\mathbf{u} = \mathbf{r}/r$. We propose an elegant algebraic technique exploiting the rank-one term $\mathbf{r}\mathbf{r}^T/r^2$ in (13). Let $\mathbf{C} = \mathbf{U}\mathbf{D}\mathbf{U}^T$ be the eigendecomposition of $\mathbf{C}$. We obtain

$$\frac{\mathbf{r}}{\|\mathbf{r}\|} \frac{\mathbf{r}^T}{\|\mathbf{r}\|} = \mathbf{U}\left[\frac{1}{3c}\mathbf{D}^{1/2} + \mathbf{I}_3\right]\mathbf{U}^T \tag{20}$$

17

which is also a rank-one matrix. Therefore, the position versor we are interested in is the eignevector $\mathbf{u}_{\max}$ corresponding to the maximum eigenvalue of $\mathbf{C}$, i.e., $\mathbf{r}/\|\mathbf{r}\| = \mathbf{u}_{\max}$. Finally the 3-D position vector can be expressed as

$$\mathbf{r} = r\mathbf{u}_{\max}. \tag{21}$$

Orientation Estimation The orientation matrix $\boldsymbol{\Omega}_{\mathrm{t}}$ can be estimated as

$$\mathbf{S} = c\boldsymbol{\Omega}_{\mathrm{t}}^T \underbrace{\left[3\mathbf{u}_{\max}\mathbf{u}_{\max}^T - \mathbf{I}_3\right]}_{\mathbf{P}}, \tag{22}$$

where $\mathbf{P} \triangleq 3\mathbf{u}_{\max}\mathbf{u}_{\max}^T - \mathbf{I}_3$ is always an invertible matrix (its eigenvalues are $\{2, -1, -1\}$). The orthogonal Procrustes problem in Eq. (22) can be solved for orthogonal $\boldsymbol{\Omega}_{\mathrm{t}}$ by polar decomposition. The polar decomposition of $c\mathbf{PS}^T = \mathbf{UH}$ is a product of an orthogonal matrix $\mathbf{U}$ and a positive semi-definite symmetric matrix $\mathbf{H}$. The nearest matrix satisfying the equality (22) under Frobenius norm is the orthogonal polar factor of $\mathbf{PS}^T, \forall c > 0$ (for details, see Higham (1989)). Therefore, the matrix describing the orientation of the RX frame in the TX frame is

$$\hat{\boldsymbol{\Omega}}_{\mathrm{t}} = s\,\mathrm{pf}\{\hat{\mathbf{P}}\hat{\mathbf{S}}^T\}, \tag{23}$$

where $\hat{\mathbf{P}} = 3\hat{\mathbf{u}}_{\max}\hat{\mathbf{u}}_{\max}^T - \mathbf{I}_3$ and $\hat{\mathbf{S}}$ is the estimated channel matrix. For a full-rank matrix $\mathbf{A}$, the polar factor can be calculated as $\mathrm{pf}\{\mathbf{A}\} \triangleq \mathbf{A}(\mathbf{A}^T\mathbf{A})^{-1/2}$. The multiplication by $s \triangleq \mathrm{sign}[\det(\mathrm{pf}\{\hat{\mathbf{P}}\hat{\mathbf{S}}^T\})]$ ensures that $\hat{\boldsymbol{\Omega}}_{\mathrm{t}}$ is a proper rotation.

Using these above relationships, the position and orientation of the receiver can be determined in 3-D, using signals from a single transmitter.

4. Multi-hop Localization

In the previous section, we showed how the receiver position and orientation can be determined for a single transmitter-receiver pair. In this section, we show how information from multiple transmitters can be fused by a single receiver for improved estimation, following the derivation presented in Abrudan et al. (2016). Assume that there are N magneto-inductive infrastructure transmitters and one receiver carried by the user. Again, we consider position and orientation estimation independently. Note, that as the system is receiver-centric, the number of receivers can be arbitrarily large.

We express the 3-D position of the receiver with respect to a transmitter in terms of a range (distance) and bearing versor (a unit vector pointing from a transmitter in the direction of the receiver). By decoupling range from bearing angle, the maximum likelihood formulation becomes conceptually simpler.

Range likelihood From Eq. (17), it follows that the likelihood of the range corresponding to the nth TX is $l_{\mathrm{r}}(r_n) = \mathcal{N}(\rho_n; \tilde{\rho}_n(r_n), \sigma_n^2)$, where ρ_n is the measured RSSI, and $\tilde{\rho}_n(r_n) = \rho_{0,n} - 60 \log_{10}(r_n/r_{0,n})$ is the RSSI predicted by the path-loss model in Eq. (17) for the range r_n.

Let $\mathbf{p}$ and $\mathbf{t}_n$ denote the position vectors in the world frame corresponding to the RX and the nth TX, respectively. Then, the range can be expressed as $r_n = \|\mathbf{p} - \mathbf{t}_n\|$. Assuming that the RSSI uncertainties are mutually independent for all N transmitters, the joint log-likelihood function including the corresponding ranges is

$$L_{\mathrm{r}}(\mathbf{p}) = c_1 - \sum_{n=1}^{N} \frac{1}{2\sigma_n^2} \left(\rho_n - \rho_{0,n} + 60 \log_{10} \frac{\|\mathbf{p} - \mathbf{t}_n\|}{r_0} \right)^2, \qquad (24)$$

19

where c_1 is a constant that does not depend on $\mathbf{p}$.

Bearing Versor Likelihood Unlike conventional range-based multilateration, we are able to estimate angles between transceivers in 3-D. In order to deal with angular uncertainties, we need probability density functions defined in a proper parameter space, that exhibits 2π-periodicity. We model the bearing versor error using von Mises-Fisher distribution, which is defined for the random 3-dimensional unit vector $\mathbf{x} \in \mathbb{R}^3$ as follows:

$$p(\mathbf{x}; \boldsymbol{\mu}, \kappa) = \frac{\kappa}{4\pi \sinh \kappa} \exp(\kappa \boldsymbol{\mu}^T \mathbf{x}), \tag{25}$$

where $\boldsymbol{\mu}$ is a unit vector pointing in the mean direction, and κ is the concentration parameter. In order to deal with the hemispherical ambiguity in position estimation which magneto-inductive positioning is subject to due to the field symmetry, we use a balanced mixture of two Fisher distributions Costa et al. (2014) whose means correspond to the estimated position versor of the nth TX $\hat{\mathbf{u}}_n = \hat{\mathbf{r}}_n/r$, and its antipodal point $-\hat{\mathbf{u}}_n$, respectively. The corresponding bimodal bearing likelihood for the nth TX is $l_\angle(\mathbf{r}) = [p(\mathbf{r}; \hat{\mathbf{u}}_n, \kappa_n) + p(\mathbf{r}; -\hat{\mathbf{u}}_n, \kappa_n)]/2$. For N transmitters, the joint log-likelihood function that includes the estimated bearing versors $\hat{\mathbf{u}}_n = (\hat{\mathbf{p}} - \mathbf{t}_n)/\|\hat{\mathbf{p}} - \mathbf{t}_n\|$ is

$$L_\angle(\mathbf{p}) = c_2 + \sum_{n=1}^{N} \ln \, \cosh \left[\kappa_n \frac{(\mathbf{p} - \mathbf{t}_n)^T}{\|\mathbf{p} - \mathbf{t}_n\|} \frac{(\hat{\mathbf{p}} - \mathbf{t}_n)}{\|\hat{\mathbf{p}} - \mathbf{t}_n\|} \right], \tag{26}$$

where c_2 is a constant that does not depend on $\mathbf{p}$. In order to set the the concentration parameter κ_n which characterizes the spread of von Mises-Fisher p.d.f., we use the eigenvalue criterion in Abrudan et al. (2015).

Joint Log-likelihood Maximization Our goal is to maximize the joint log-likelihood corresponding to the N TXs that includes range and 3-D bear-

ing information $L(\mathbf{p}) = L_{\mathrm{r}}(\mathbf{r}) + L_{\angle}(\mathbf{r})$, and this is achieved by using a steepest ascent algorithm. Fig. 1 shows that the joint range and bearing likelihood function has a well-defined maxima in the vicinity of the true position.

Using the derived maximum likelihood, it is possible now to find the best position estimate of the receiver. Using a multi-hop configuration allows for scalable and more precise positioning, as the range limitations caused by the inverse cube law path loss are overcome.

5. Applications of Underground MI positioning

In this section, we present two examples of how MI can be used to provide through-earth positioning capability. We discuss how MI can be used to form an iteratively deployable multi-hop positioning infrastructure, suitable for rescue situations and how MI can be used to precisely track the locations of burrowing animals underground.

5.1. Iteratively Deployable Positioning Architecture

In an underground rescue situation, such as a mining collapse or caving accident, it is necessary to have accurate positioning of rescue team members (which could be people or even robotic agents). However, valuable time cannot be wasted setting up a positioning system. A novel, iterative, positioning system is presented in Abrudan et al. (2016) as a proof-of-concept. The key idea is that a single anchor node is placed at a known location (such as a tunnel entrance) to act as the origin. The receiver is localized relative to the transmitter. However, this faces the issue that positioning range is limited by the coverage of the first transmitter. To extend the range, additional transmitters can be deployed. The receiver, using the first transmitter as the

origin, can localize the additional transmitters and subsequently use them as anchors when outside the range of the original anchor. In this way, a positioning system can be iteratively deployed, without requiring any additional surveying effort or worrying about anchor geometry as would be the case in range based systems.

The outline of the main phases in this approach is discussed as follows: **Phase I:** In this initial phase, receivers localize themselves relative to the transmitter at the origin (TX1).

Phase II: In this phase, to maintain coverage, receivers derive the location of the additional transmitter(s) (TX2 in this case) with respect to the origin.

Phase III: Positions of the receiver is then estimated with all the transmitters using a maximum likelihood approach.

We carried out experiments in a man-made cave within a space of $15 \times 15 \times 2$ meters^3, with a schematic layout shown in Fig. 2. It is well-known that accurately mapping underground caves in 3-D is an extremely difficult and time-consuming task. Ground truth locations were surveyed using laser-based range and inclination meters. The origin was set closer to the cave entrance, such that its global position can be inferred easily. The transmitter TX1 was placed at the origin and acted as a primary anchor, and secondary anchor TX2 was placed in a different tunnel. Note that the tunnels were not planar, they exhibit a difference in elevation of approximately 2 meters.

The two transmitters were equipped with square triaxial coils (30 cm side and 80 turns), similar to Markham and Trigoni (2012a). The receiver contains small triaxial coils (around 20 mm long) and an IMU for gravity vector estimation. The system transmitted vector modulated signals at a

frequency of 2.5 kHz, with a bandwidth of 31.25 Hz and a code length of 36 symbols.

The experiment was carried out close to the origin (see Fig. 3)(a). A measuring tape was laid on the ground and magneto-inductive measurements were collected from two different transmitters (TX1 acting as single anchor, and TX2 shown in green), every two meters along the tape (points t1 to t7 in magenta color). The surveyed receiver 3-D positions and orientations are shown in Fig. 3(a) by the magenta dots and frames, respectively. The subsequent relative receiver orientations were with the x-axis parallel to the tape, pointing in the direction opposite to the origin, and the z-axis pointing down. Fig. 3 shows the three phases of the network deployment and discovery algorithm.

Phase I is shown in Fig. 3(b), where the receiver 3-D positions and orientations are estimated using TX1 only as an anchor. The hemispherical ambiguity was removed with the basic knowledge that the measured locations are on the positive side of the y-axis of the anchor TX1. The orientation ambiguity was removed based on the gravity vector, which was estimated from the RX inertial measurement unit.

Phase II is depicted in Fig. 3(c), where two estimated receiver 3-D positions and orientations are used as virtual anchors in order to estimate the position and the orientation of TX2.

Phase III is shown in Fig. 3(d). The newly discovered anchor TX2 is used to estimate the receiver 3-D positions and orientations, in tandem with TX1 when available.

In terms of receiver positioning accuracy, the estimation approach pro-

vides a very reliable estimate, the positioning errors are well below 1 meter for most of the locations and orientation estimation errors remain below 10 degrees. Although the scale of the proof-of-concept trial is small, it demonstrates the fundamentals of accurate 3-D positioning through solid rock. In addition, the use of multiple deployable secondary anchors allows the system to scale gracefully. In summary, this technique could find great use in underground rescue, autonomous mining and cave exploration.

5.2. Revealing Underground Animal Behaviour

Many animals spend a large proportion of their lives underground in burrows or dens, to provide safety and refuge. Due to a lack of non-invasive technologies which can determine where they precisely are underground, little has been known about their detailed activity. This is especially important for animals such as badgers (*Meles meles*) which live in large, communal underground burrows which can house up to 20 animals over a few hundred square metres (see Noonan et al. (2015)). To address this problem, a low power MI tracking technology was developed. This comprised three core components: the transmitting antennas, placed above the area to be monitored; the tracking collars, worn by the study animals; and the above-ground basestation which wirelessly received buffered data when animals emerged to forage every night, as described in Markham et al. (2010).

The transmitting antennas are time multiplexed and emit unique digital codes, modulated with amplitude-shift-keying. They are large (2m × 15m) rectangular loops of cable that are dug into the ground to provide long-term robustness (for details, see Markham and Trigoni (2012b)). Typically 8 antennas arranged in an X-Y matrix are used to provide sufficient spatial

24

coverage.

The collars comprise a low power microcontroller, an analog triaxial MI sensor, a flash memory, 802.15.4 wireless transceiver and are powered by a small lithium cell. The MI sensor listens for an encoded signal from each antenna, and converts this measurement to a single RSSI value. By using three orthogonal sensors, the orientation of the collar, which is unknown, becomes an invariant. The RSSI values from all the transmitting antennas are stored and time-stamped in the onboard flash memory. The radio transceiver periodically tries to establish a link with the basestation, which typically occurs when an animal emerges every night to forage. The device then reliably transfers the stored data to the basestation, ready for post-processing.

To determine the animal's trajectory, a model of the magnetic field generated by each transmitting antenna is used. These are simple geometric structures, so application of Biot-Savart's Law allows for the magnetic field strength to be readily calculated using the method presented by Misakian (2000). A particle filter is then used to estimate the animal's location, given the MI field readings and knowledge of the antenna geometry. Typical accuracies of 30 cm RMS error in 3-D are obtained, allowing for extremely precise tracking of underground animal movement, as shown in Fig. 4. With a high temporal sampling rate of 0.3 Hz, it is possible to obtain detailed trajectories of animal movements, both above and below ground, as can be seen in Fig. 5. Lastly, one of the major advantages of such a system is that over time it not only tracks animal movements, but as animals are constrained to move within their burrows, also reveals their underground tunnel structure, shown in Fig. 6.

In summary, a low-power MI positioning system was used to provide highly accurate GPS-like positioning of a number of animals simultaneously. This in turn has helped to uncover new biological findings about how animals interact underground and what the precise function of their burrows is (see Noonan et al. (2015) for more details).

6. Challenges and limitations

6.1. Path loss

While magnetic induction-based communication and positioning systems have the aforementioned advantages of low attenuation in dense media, and the ability to use the vector field for positioning, they suffer from inherent physical limitations.

One of those limitations is path loss; the magnetic field of a magnetic dipole in the near-field region decays with the inverse cube of the distance, such that $H(r) \propto r^{-3}$, corresponding to a path loss of 60 dB per decade. In contrary, the magnetic field of a Hertzian dipole radiating in the far-field region decays as $H(r) \propto r^{-1}$ Jin (2010), corresponding to a path loss of only 20 dB per decade.

To compensate for a high path loss, magnetoinductive transmitters have to comprise of bulky coils able to carry large amounts of current, and receivers of highly sensitive coils with a very low noise floor, able to sense tiny fields. For communication, sophisticated signal processing techniques must be used to make the most of the limited bandwidth.

In designing a transmitter with a particular environment in mind, path loss is a major concern. More specifically, there are two major factors that

must be taken into account: a) the physical configuration/geometry of the field source, and b) the material properties of the medium the field is established in, or propagating through.

The first factor becomes important especially in the near field, where the decay does not solely follow an inverse power law, but has multipole terms, which become more significant as one approaches the source. These decay terms are independent of material properties and frequency, and only depend on the distance.

An additional type of attenuation comes into effect when the medium is electrically conductive or magnetically permeable, or when the frequency is high, or both. This type of attenuation does not follow an inverse power law, but instead is exponential in nature. The attenuation constant, usually denoted as α, is what determines the rate of decay, and it is a function of material properties as well as operating frequency. A general expression for α is given by Jordan and Balmain (1968):

$$\alpha = \omega \sqrt{\frac{\mu\epsilon}{2} \left(\sqrt{1 + \frac{\sigma^2}{\omega^2 \epsilon^2}} - 1 \right)} \tag{27}$$

where ω is the angular frequency, μ is the magnetic permeability, ϵ is the electric permittivity, and σ is the electrical conductivity. One may notice that indeed, α increases with frequency, electrical conductivity, and magnetic permeability. When considering conducting objects, $\epsilon = 1$ and (27) simplifies to

$$\alpha = \sqrt{\frac{\sigma \omega \mu}{2}}, \tag{28}$$

27

where $\delta = 1/\alpha$ is the well known skin depth.

6.2. Distortion due to nearby conducting objects

Electrically conducting objects significantly obstruct electromagnetic fields and can pose a problem in communication and positioning. In the far-field one can assume plane wave propagation, which greatly increases mathematical tractability when calculating reflection and scattering from objects. This assumption is valid when the distance of the observation point from the source is much larger than the wavelength of the radiated electromagnetic wave, which causes the electric and magnetic fields of the wave to be mutually orthogonal. In the near-field, where the distance from the source is comparable to the wavelength such that the source geometry matters, this approximation is not valid, and one does not commonly find closed form solutions that describe reflections from conducting objects, even for simple geometries.

In general, the flux density generated by the transmitter induces eddy currents within the conductors, which then radiate a secondary (scattered) flux density. If the eddy-currents can be classified as inductance limited Hammond (1962), the surfaces of the conductors behave as if they were perfect electric conductors (PEC), and the magnetic field in their vicinity is as if the conductors had zero magnetic permeability (the flux density normal to the surface is close to zero). The total flux density $\mathbf{B}^{\mathrm{t}}$ outside the conducting regions will then be equal to

$$\mathbf{B}^{\mathrm{t}} = \mathbf{B}^{\mathrm{i}} + \mathbf{B}^{\mathrm{s}}, \tag{29}$$

where $\mathbf{B}^i$ is the incident flux density due to the point dipole and $\mathbf{B}^s$ is the scattered flux density due to re-radiation by the conducting objects.

One way to model the scattered flux density and obtain an expression for the total field $\mathbf{B}^t$ is to use image theory. In image theory, the conducting object is replaced with an image of the dipole, and the sum of the real and imaginary dipoles gives the total field Kypris et al. (2015).

The way to autonomously combat the problem of distortions due to conducting objects, is to 1) recognize that the field does not behave as expected, 2) switch to a different channel model that takes into account these objects. The former can be achieved by assessing the symmetry of the dipole field. In the presence of conducting material, the energy is redistributed among different axes (while preserved in total), thus changing the symmetry of the field. Knowledge of this can be used to switch to a different channel model that takes into account these distortions Abrudan et al. (2015).

7. Conclusion

As has been outlined, magneto-inductive technology has certain unique advantages that make it ideal for communication and location through many different media, ranging from concrete and soil to people and air. It does not suffer from boundary effects like acoustic and seismic technology, nor is it prone to multipath fading like RF techniques. MI positioning has enabled tracking of objects in environments where before it was difficult or even impossible. However, it does have a number of disadvantages, the most significant being the limited range due to rapid path loss. This fundamentally curtails its maximum achievable range. With advances in sensor technology

however, leading to miniature, solid state magnetic sensors that can approach super cooled SQUIDs, there is certainly a bright future for this MI.

References

Abrudan, T. E., Xiao, Z., Markham, A., Trigoni, N., Nov. 2015. Distortion rejecting magneto-inductive three-dimensional localization (MagLoc). IEEE Journal on Selected Areas in Communications 33 (11), 2404–2417.

Abrudan, T. E., Xiao, Z., Markham, A., Trigoni, N., Aug. 2016. Underground, incrementally deployed magneto-inductive 3-D positioning network. IEEE Transactions on Geoscience and Remote Sensing 54 (8), 4376–4391.

Barkand, T., Damiano, N., Shumaker, W., Oct 2006. Through-the-earth, two-way, mine emergency, voice communication systems. In: Industry Applications Conference, 2006. 41st IAS Annual Meeting. Conference Record of the 2006 IEEE. Vol. 2. pp. 955–958.

Bedford, M., Kennedy, G., May 2012. Evaluation of zigbee (ieee 802.15.4) time-of-flight-based distance measurement for application in emergency underground navigation. Antennas and Propagation, IEEE Transactions on 60 (5), 2502–2510.

Costa, M., Koivunen, V., Poor, H. V., Dec. 2014. Estimating directional statistics using wavefield modeling and mixtures of von-Mises distributions. IEEE Signal Processing Letters 21 (12), 1496–1500.

Cypriani, M., Delisle, G., Hakem, N., 2015. Wi-fi-based positioning in a complex underground environment. Journal of Networks 10 (3).

Hammond, P., 1962. The calculation of the magnetic field of rotating machines. part 3: eddy currents induced in a solid slab by a circular current loop. Proceedings of the IEE-Part C: Monographs 109 (16), 508–515.

Haverinen, J., Kemppainen, A., Sept 2011. A geomagnetic field based positioning technique for underground mines. In: Robotic and Sensors Environments (ROSE), 2011 IEEE International Symposium on. pp. 7–12.

Hawkins, W., Daku, B., Prugger, A., Nov 2006. Positioning in underground mines. In: IEEE Industrial Electronics, IECON 2006 - 32nd Annual Conference on. pp. 3139–3143.

Higham, N. J., 1989. Matrix nearness problems and applications. In: Gover, M. J. C., Barnett, S. (Eds.), Applications of Matrix Theory. Oxford University Press, pp. 1–27.

Huang, X., Zhu, W., Lu, D., 2010. Underground miners localization system based on zigbee and webgis. In: Geoinformatics, 2010 18th International Conference on. IEEE, pp. 1–5.

Hummel, J. B., Bax, M. R., Figl, M. L., Kang, Y., Maurer, C., Birkfellner, W. W., Bergmann, H., Shahidi, R., 2005. Design and application of an assessment protocol for electromagnetic tracking systems. Medical Physics 32 (7), 2371–2379.

International Commission on Non-Ionizing Radiation Protection, 2010. Guidelines for limiting exposure to time-varying electric and magnetic fields (1 Hz to 100 kHz). Health Physics 99 (6), 818–836.

Jin, J.-M., 2010. Theory and computation of electromagnetic fields. Wiley, Hoboken and N.J.

Jordan, E. C., Balmain, K. G., 1968. Electromagnetic Waves and Radiating Systems. Vol. 4. Prentice-Hall, Englewood Cliffs, NJ.

Kindratenko, V., 2000. A survey of electromagnetic position tracker calibration techniques. Virtual Reality 5 (3), 169–182.

Kypris, O., Abrudan, T. E., Markham, A., 1–4 Nov. 2015. Reducing magneto-inductive positioning errors in a metal-rich indoor environment. In: IEEE Sensors Conference. pp. 1–4.

Markham, A., Trigoni, N., 2012a. Magneto-inductive networked rescue system (MINERS): taking sensor networks underground. In: "11th International Conference on Information Processing in Sensor Networks (IPSN 2012).

Markham, A., Trigoni, N., June 2012b. Underground localization in 3-D using magneto-inductive tracking. IEEE Sensors Journal 12 (6), 1809–1816.

Markham, A., Trigoni, N., Ellwood, S. A., Macdonald, D. W., Nov. 2010. Revealing the hidden lives of underground animals using magneto-inductive tracking. In: 8th ACM Conference on Embedded Networked Sensor Systems (Sensys 2010). Zürich, Switzerland.

Misakian, M., 2000. Equations for the magnetic field produced by one or more rectangular loops of wire in the same plane. Journal Of Research-National Institute Of Standards And Technology 105 (4).

Nkakanou, B., Delisle, G. Y., Hakem, N., 2011. Experimental characterization of ultra-wideband channel parameter measurements in an underground mine. Journal of Computer Networks and Communications 2011.

Noonan, M. J., Markham, A., Newman, C., Trigoni, N., Buesching, C. D., Ellwood, S. A., Macdonald, D. W., 2015. A new magneto-inductive tracking technique to

uncover subterranean activity: what do animals do underground? Methods in Ecology and Evolution 6 (5), 510–520.

Park, B., Myung, H., 2014. Underground localization using dual magnetic field sequence measurement and pose graph slam for directional drilling. Measurement Science and Technology 25 (12), 125101.

Pfeil, R., Pichler, M., Schuster, S., Hammer, F., Nov 2015. Robust acoustic positioning for safety applications in underground mining. Instrumentation and Measurement, IEEE Transactions on 64 (11), 2876–2888.

Raab, F., Blood, E., Steiner, T., Jones, H., Sept. 1979. Magnetic position and orientation tracking system. Aerospace and Electronic Systems, IEEE Transactions on AES-15 (5).

Shaffer, G., Stentz, A., Whittaker, W., Fitzpatrick, K., Sep 1992. Position estimator for underground mine equipment. Industry Applications, IEEE Transactions on 28 (5), 1131–1140.

Silva, A., Vuran, M., 2009. Empirical Evaluation of Wireless Underground-to-Underground Communication in Wireless Underground Sensor Networks. In: Proceedings of the 5th IEEE International Conference on Distributed Computing in Sensor Systems.

Squire, J., Sullivan, G., Baker, E., Flathers, G., 2009. Proof-of-concept testing of a deep seismic communication device. Society for Mining, Metallurgy, and Exploration 326, 97–100.

Stolarczyk, L. G., Jul 1991. Emergency and operational low and medium frequency band radio communications system for underground mines. Industry Applications, IEEE Transactions on 27 (4), 780–790.

Stuntebeck, E., Pompili, D., Melodia, T., 2006. Underground wireless sensor networks using commodity terrestrial motes. Tech. rep., Georgia Institute of Technology.

Sun, Z., Akyildiz, I., July 2010. Magnetic induction communications for wireless underground sensor networks. Antennas and Propagation, IEEE Transactions on 58 (7), 2426–2435.

Telford, W. M., Geldart, L. P., Sheriff, R. E., 1990. Applied Geophysics (2nd edition). Cambridge University Press.

Tumanski, S., 2007. Induction coil sensorsa review. Measurement Science and Technology 18 (3), R31.

Wadley, T., 1946. Underground communication by rocks in gold mines on the witwaterrand. South Africa wet. Ny-werheid-Navorsingsraad, Johannesburg, South Africa, Telekommunikasies Navorsing Laboratorium TRL.

Yarkan, S., Guzelgoz, S., Arslan, H., Murphy, R., rd 2009. Underground mine communications: A survey. Communications Surveys Tutorials, IEEE 11 (3), 125–142.

List of Figures

Figure 1: Illustration of the joint range-bearing likelihood function for two transmitters TX1 and TX2. The two spheres correspond to the most likely ranges. The joint likelihood is maximized close to the true RX position (shown by the black dot).
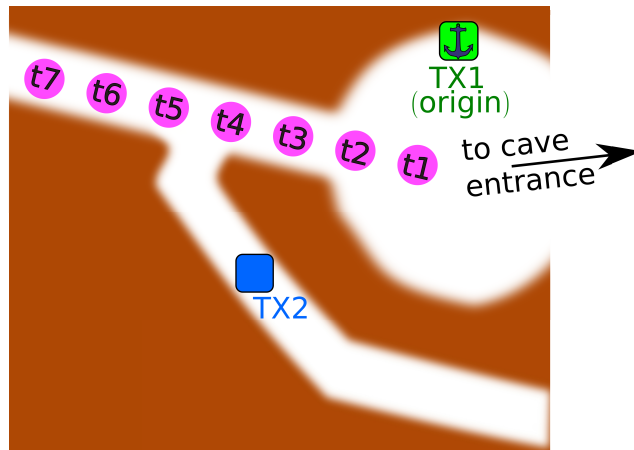
Figure 2: 2-D schematic layout of cave system, showing surveyed anchor transmitter (TX1), secondary transmitter at unknown position (TX2) and test points (t1–t7) where the receiver is localized. Note that there are no line-of-sight paths between either transmitter and the test points, or between the two transmitters.
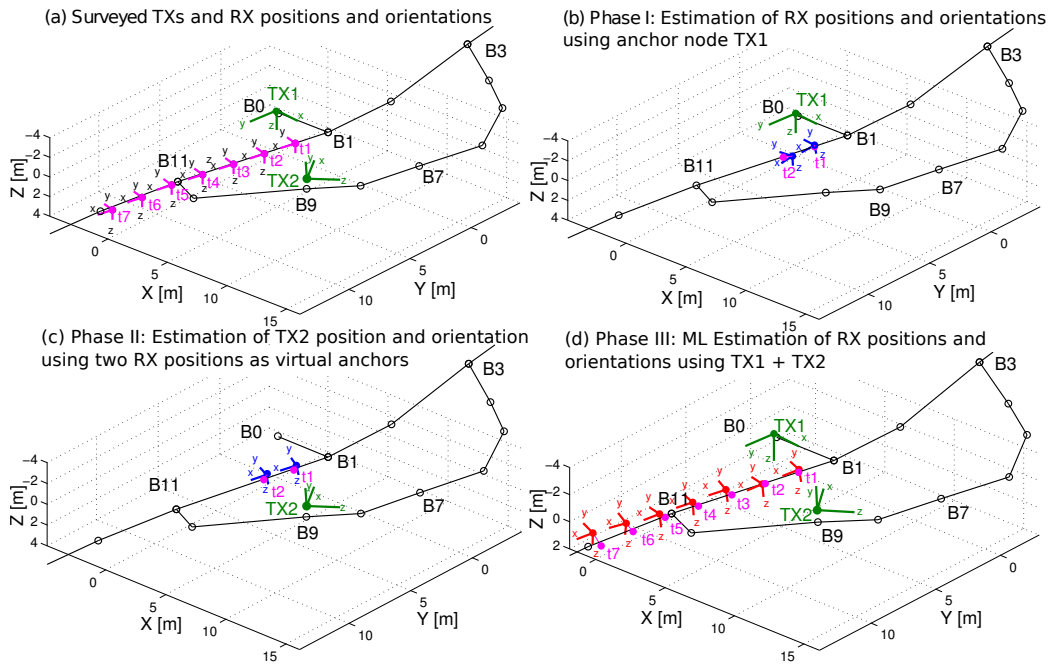
Figure 3: Linear displacement experiment. The surveyed positions and orientation of TX1 and TX2 are shown in green. (a) Surveyed RX positions and orientations t1–t7 are shown in magenta color. (b) Phase I: Two estimated RX 3-D positions and orientations using TX1 as anchor node. (c) Phase II: Estimated TX2 position and orientation using the two previously estimated RX positions and orientations as virtual anchors. (d) Phase III: Estimated RX positions and orientations using ML and both TX1 and TX2.

38
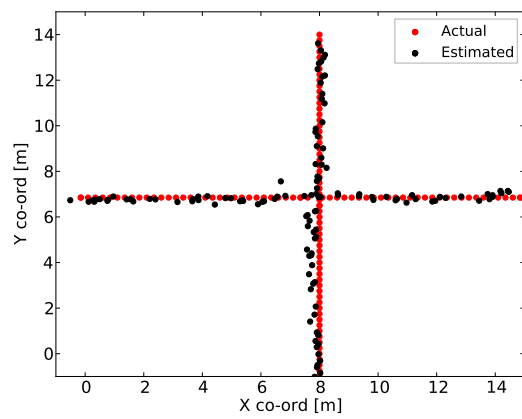
Figure 4: Plot showing 2-D positioning accuracy of underground animal tracking system
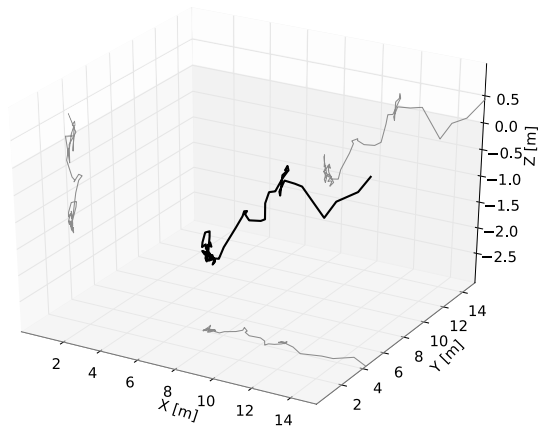
Figure 5: Detailed trajectory showing animal emerging from below ground to above ground
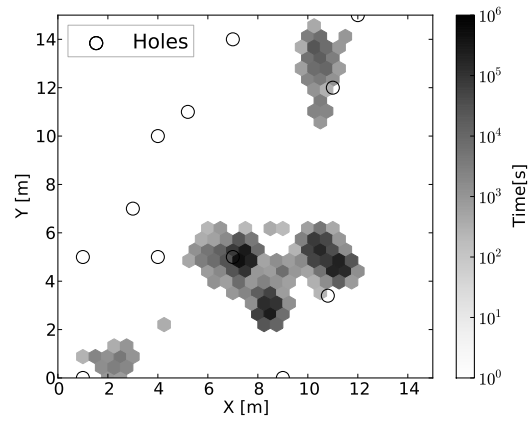
Figure 6: History of animal movements over many weeks reveals their underground burrow structure
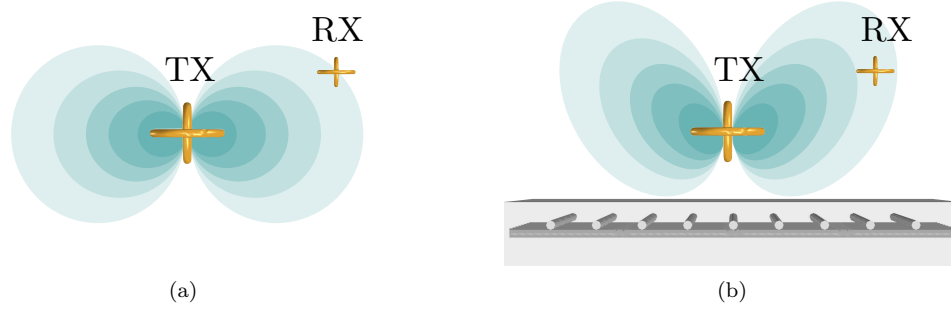
Figure 7: Representation of the magnetic field distribution of a magneto-inductive system, depicting a triaxial coil transmitter and receiver a) in free space, and b) over an array of metallic objects, which perturb the field symmetry Kypris et al. (2015).